

Lecture Notes in Mechanical Engineering

Gujjala Raghavendra
B. B. V. L. Deepak
Manoj Gupta *Editors*

Recent Advances in Mechanical Engineering, Volume 2

Select Proceedings of ICMech-REC 23

 Springer

Lecture Notes in Mechanical Engineering

Series Editors


Fakher Chaari, National School of Engineers, University of Sfax, Sfax, Tunisia

Francesco Gherardini , Dipartimento di Ingegneria “Enzo Ferrari”, Università di Modena e Reggio Emilia, Modena, Italy

Vitalii Ivanov, Department of Manufacturing Engineering, Machines and Tools, Sumy State University, Sumy, Poland

Mohamed Haddar, National School of Engineers of Sfax (ENIS), Sfax, Tunisia

Editorial Board

Francisco Cavas-Martínez , Departamento de Estructuras, Construcción y Expresión Gráfica Universidad Politécnica de Cartagena, Cartagena, Spain

Francesca di Mare, Institute of Energy Technology, Ruhr-Universität Bochum, Bochum, Germany

Young W. Kwon, Department of Manufacturing Engineering and Aerospace Engineering, Graduate School of Engineering and Applied Science, Monterey, USA

Tullio A. M. Tolio, Department of Mechanical Engineering, Politecnico di Milano, Milano, Italy

Justyna Trojanowska, Poznan University of Technology, Poznan, Poland

Robert Schmitt, RWTH Aachen University, Aachen, Germany

Jinyang Xu, School of Mechanical Engineering, Shanghai Jiao Tong University, Shanghai, China

Lecture Notes in Mechanical Engineering (LNME) publishes the latest developments in Mechanical Engineering—quickly, informally and with high quality. Original research or contributions reported in proceedings and post-proceedings represents the core of LNME. Volumes published in LNME embrace all aspects, subfields and new challenges of mechanical engineering.

To submit a proposal or request further information, please contact the Springer Editor of your location:

Europe, USA, Africa: Leontina Di Cecco at Leontina.dicecco@springer.com

China: Ella Zhang at ella.zhang@springer.com

India: Priya Vyas at priya.vyas@springer.com

Rest of Asia, Australia, New Zealand: Swati Meherishi at swati.meherishi@springer.com

Topics in the series include:

- Engineering Design
- Machinery and Machine Elements
- Mechanical Structures and Stress Analysis
- Automotive Engineering
- Engine Technology
- Aerospace Technology and Astronautics
- Nanotechnology and Microengineering
- Control, Robotics, Mechatronics
- MEMS
- Theoretical and Applied Mechanics
- Dynamical Systems, Control
- Fluid Mechanics
- Engineering Thermodynamics, Heat and Mass Transfer
- Manufacturing Engineering and Smart Manufacturing
- Precision Engineering, Instrumentation, Measurement
- Materials Engineering
- Tribology and Surface Technology

Indexed by SCOPUS, EI Compendex, and INSPEC.

All books published in the series are evaluated by Web of Science for the Conference Proceedings Citation Index (CPCI).

To submit a proposal for a monograph, please check our Springer Tracts in Mechanical Engineering at <https://link.springer.com/bookseries/11693>.

Gujjala Raghavendra · B. B. V. L. Deepak ·
Manoj Gupta
Editors

Recent Advances in Mechanical Engineering, Volume 2

Select Proceedings of ICMech-REC 23

 Springer

Editors

Gujjala Raghavendra
Department of Mechanical Engineering
National Institute of Technology Warangal
Warangal, Telangana, India

B. B. V. L. Deepak
Department of Industrial Design
National Institute of Technology Rourkela
Rourkela, Odisha, India

Manoj Gupta
Department of Mechanical Engineering
National University of Singapore
Singapore, Singapore

ISSN 2195-4356

ISSN 2195-4364 (electronic)

Lecture Notes in Mechanical Engineering

ISBN 978-981-97-2248-8

ISBN 978-981-97-2249-5 (eBook)

<https://doi.org/10.1007/978-981-97-2249-5>

© The Editor(s) (if applicable) and The Author(s), under exclusive license to Springer Nature Singapore Pte Ltd. 2024

This work is subject to copyright. All rights are solely and exclusively licensed by the Publisher, whether the whole or part of the material is concerned, specifically the rights of translation, reprinting, reuse of illustrations, recitation, broadcasting, reproduction on microfilms or in any other physical way, and transmission or information storage and retrieval, electronic adaptation, computer software, or by similar or dissimilar methodology now known or hereafter developed.

The use of general descriptive names, registered names, trademarks, service marks, etc. in this publication does not imply, even in the absence of a specific statement, that such names are exempt from the relevant protective laws and regulations and therefore free for general use.

The publisher, the authors and the editors are safe to assume that the advice and information in this book are believed to be true and accurate at the date of publication. Neither the publisher nor the authors or the editors give a warranty, expressed or implied, with respect to the material contained herein or for any errors or omissions that may have been made. The publisher remains neutral with regard to jurisdictional claims in published maps and institutional affiliations.

This Springer imprint is published by the registered company Springer Nature Singapore Pte Ltd.

The registered company address is: 152 Beach Road, #21-01/04 Gateway East, Singapore 189721, Singapore

Paper in this product is recyclable.

Contents

Structural, Mechanical, and Corrosion Resistance Properties in 3.5% NaCl Solution of Electroless Deposited Ternary Ni–P–W System	1
Muralidharan Ramachandran, Pranay Vagad, Ramavtar Sharma, P. P. Deshpande, Ravi Bhatkal, and Dinesh Semwal	
Dry Ice Cooling Effect on Friction Stir Welded AA6061 Alloy Using Brass Interlayer	15
Korra Nagu and Adepu Kumar	
An Investigation of Compaction Pressure on Tribological and Mechanical Properties of Powder Metallurgy-Based Non-equiatomic High Entropy Alloy	29
Abhishek Samaniya, Deepak Kumar Chandel, Lalit Thakur, and Vinod Kumar	
Development of Coupled Double Ellipsoid Heat Source Model for Hybrid Laser TIG Welding of Thick Steel Plate	41
M. S. Sumanlal, N. S. Sivasubramanian, and V. M. Joy Varghese	
Influence of Chemical Treatment on the Microstructural Properties of <i>Sida acuta</i> Natural Fiber	55
H. Jeevan Rao, Dheeraj Kumar Gara, Saranya Reddy, V. R. Shreya, Tarun Kumar, Edel Sequeria, and Ayush Jha	
Experimental Study of Temperature Distribution and Oil Flow Rate for Plain and Herringbone-Grooved Hydrodynamic Journal Bearing	65
Nitin Borse, Harsh Sonavane, Akshit Shinde, and Shriniwas Chippha	
Machine Learning-Based Prediction of Butanol–Diesel Dual Fuel Engine Performance and Emissions	77
Anil Kumar Alli, Nayan Pramod Vilhekar, and Madhu Murthy Kotha	

Modification of Lateritic Soil Used as Bricks with Banana Leaves Ash	93
Idayat Oluwakemi Sholadoye, Bitrus Emmanuel Achara, and Bridget Orekwu Ojobo	
Comprehensive Analysis of Laser Processing Parameters on SS304 Steel: Experimental and Mathematical Insights	105
Vishal K. Shrirame and Harendra Kumar Narang	
Friction-Stir-Surfacing (FSS) Process of Aluminum Alloy (AA6061) Coating Over Mild Steel (IS2062) Substrate	115
A. Naresh, K. Veera Venkata Nagaraju, G. Venkatesh, and B. Vijaya Kumar	
Multi-objective Optimization of Graphite Powder Mixed Electric Discharge Machining Process Parameters on Inconel 625 Using Genetic Algorithm	127
Gangadharudu Talla, M. Muniraju, and Shaik Saida Vali	
Numerical Modeling of Skin Bioheat Transfer Using Finite Difference Method	141
Dulam Naveen Reddy, K. Spandana Bhat, Polinati Rajesh, Ramavath Krishna Kishore, Chappa Abhiram, and Ranjith Maniyeri	
Energy and Exergy Analyses of Vortex Tube Coupled Vapour Compression Refrigeration Cycle	151
Rashin Khera, Akhilesh Arora, and B. B. Arora	
Cladding of Mild Steel Plates Using CMT Process	163
Varsha Mishra, N. Yuvaraj, and Vipin	
Optimization of Machining Parameters of Niobium C-103 Using Taguchi and ANN Techniques	173
Kotha Aravind Sankeerth, T. Karthikeya Sharma, and Ch. Surya Prakash Rao	
Study of Sand Particle Erosive Wear Behavior of Advanced Aluminum Matrix Composites	187
Chittibabu Golla, R. Narasimha Rao, Syed Ismail, and Mahammad Babar Pasha	
Experimental Analysis on FDM-3D Printing Process Parameters Optimization to Enhance Tensile Strength with PLA Material	197
R. Raffik, K. Akila, B. Sabitha, J. Sivaguru, C. Naveen, and A. Sakira Parveen	

Hardness and Compressive Properties on Metal Matrix Composites with Influence of Nano-Ceramic Particles Through Powder Metallurgy Process 207
 N. Bhuvaneshwari, Muthusamy, Ravikiran Kamath Billady, S. Balakrishnan, B. Marxim Rahula Bharathi, and L. Vadivukarasi

Overview of Ample Investigation on Renewable Energy Sources: Types of Sources, Tasks, and Implications: A Review 221
 V. Senthil Murugan, Hassan Majeed Hassoon ALDelfi, Kaushal Kumar, S. S. S. V. Gopala Raju, Sumanth Ratna Kandavalli, and Pradeep Johnson

Microhardness and Wear Rate Analysis on Laser Cladded Composites of AZ91D Alloy with SiC by Grey Technique 235
 L. Karthick, Ganesh Babu Loganathan, C. A. Jagadish, B. Somasundaram, Sumanth Ratna Kandavalli, and P. Chithambaranathan

Robopill for Enhanced Drug L-Carnitine Delivery in the Gastrointestinal Tract 251
 Vikram Vinayakrao Nimbalkar, Niraj S. Vyawahare, Manoj Maruti Jagdale, and Pandurang M. Gaikwad

Simulation of Heat Stratification in Thermal Energy Storage Tank Using Fluent 259
 Gujjar Naga Malleswara Rao and Shaik Chand Mabhu Subhani

Comprehensive Study of Phase Change Materials for Solar Thermal Energy Storage 273
 Nimmani Venkata Narasimha Rao, N. Alagappan, and CH. V. K. N. S. N. Moorthy

Biofunctionalized Nanomaterials for Bioremediation of Pollutants 283
 Manne Anupama Ammulu, Kanaka Durga Devi Nelluri, Naga Sai Satya Sree Rechamalla, Naga Velangani Sai Sree Rechamalla, and Tanvitha Vadlamudi

Anchoring Silver Nanoparticles by Papaya Fruit Extract: An Efficient, Economic and Environment-Friendly Approach 293
 Kanaka Durga Devi. Nelluri, Jaladi Bhagavan, Vaka Koti Reddy, Kundurthi Surendra, and Sahithi Kamepalli

Pre-detection of Fire Accidents in Locomotive with Microcontroller 301
 Mallapuram Bala Chennaiah, G. Dilli Babu, K. Dilip Kumar, P. Nanda Kumar, and M. Sivarama Krishnaiah

Microstructural and Mechanical Properties of Friction Stir Welded (FSW) AA7075 with B₄C Reinforcement	309
Ch. Kishore Reddy, Chitrada Prasad, K. Sri Ram Vikas, M. Srinivasa Reddy, and Rahul	
Hygrothermal Impact on Mechanical Behavior of Carbon T300 and S-Glass Hybrid Fiber-Reinforced Composites Under Various Stacking Sequences	317
E. Kavitha, K. Sivaji Babu, and M. R. S. Satyanarayana	
Two-Body Abrasive Wear of Alumina and Alumina-Graphene Composite Ceramic Material: Effect of Speed and Sliding Distance	329
K. I. Vishnu Vandana, M. Rajyalakshmi, P. Phani Prasanthi, and P. Siva Nagasree	
Estimation of Mechanical and Thermal Properties of Glass and Sisal Fiber Composites with Polyester Resin Matrix	337
K. Venkatarao, Ch. Lakshmi Kanth, A. Venkata Jayasri, Ch. Mani Kishore, and B. Chaitanya	
Collaborative Learning Robots	349
P. Venu Madhav, U. Koteswara Rao, A. Yogitha, and V. Subba Reddy	
Modelling and Stress Analysis of Aerospace Bracket Using Abaqus	361
Praveen Chapala, Shivanand Jha, V. J. Harry Asher, CH. B. V. S. S. Ram Raj, and Ajay Sirra	
Experimental Investigation on Combined ABS and PLA Materials Using 3D Printing FDM Machine	371
M. Sumalatha, B. Supraja Reddy, M. B. Chennaiah, Shaik Shoaib, and V. V. S. Kesava Rao	
Development and Characterization of Nanofiller-Reinforced PLA Composites for Biodegradable Bone Fracture Fixation Devices	383
N. Ranganath, A. Ramesh, T. R. Girish, A. Hareesh, and H. V. Panchakshari	
Mechanical Behavior of Poly Lactic Acid (PLA)-Based Composites Reinforced with Alloy Wires	397
N. Ranganath, A. Hareesh, A. Ramesh, D. Harsha Vardhan, and T. R. Girish	
Mechanical Characterization of Hybrid GFRP with Alumina (Al₂O₃) Filler	413
D. Harsha Vardhan, K. Manohar Reddy, Y. Santhosh Kumar Reddy, A. Chandra Babu, and Srikar Potnuru	

Prediction of Process Parameters in CNC Milling of Natural Composites 421
 B. Anjaneyulu, R. Meenakshi Reddy, D. Sai Chaitanya Kishore, Hariprasad Tarigonda, and Sandhya Rani Borukati

Static Stress Analysis of Dental Crown with Different Materials Using Finite Element Approach 431
 I. Ramu, J. Chandra Sekhar, N. V. V. Manikanta, M. Venu, and N. Malleswararao Battina

Influence of Track Width, Wheel Base on Turning Radius and Static Behavior of Stub Axle, C-Clamp in Go-Karts Steering System 441
 Jay Prakash Srivastava, Kavvempally Suryateja, Pankaj Kumar, Gankidi Gangadhar Reddy, Mohammed Moizuddin, Subodh Kumar, and Amit Kumar Jain

Air Jet Impingement Cooling Over a Thick Flat Plate 451
 Vikash Kumar Singh Chauhan and Pankaj Kumar

Evaluation of Mechanical Properties of Various Fiber Reinforced 3D Printed Composites 459
 Pankaj Kumar, Syed Faisal Nouman, and Manowar Hussain

Prediction of Future Sales Using Machine Learning Algorithms 471
 Shashi Kumar Bharti, Santosh Kr. Mishra, S. Silva Sajin Jose, and Purushottam Kumar Singh

An Environmental Sensitive Approach to Reusable Waste Heat Using Combined Low-Temperature Water Heating-Thermoelectric Generation System 481
 Samarjeet Kumar, Swaroop Kumar Mandal, Purushottam Kumar Singh, Santosh Kr. Mishra, and Pankaj Kumar

Evaluation of Mechanical Properties of a Crab Shell Hybrid Composite 489
 G. Narasinga Rao, L. Daloji, D. Revanth, and I. Ramu

A Response Surface Methodology-Based Optimization to Realize the Correlation Between Constituent Composition of the Composite 501
 Naveen Kumar Rajendran and Amalesh Barai

Processing and Characterizations of Ferrite Incorporated PVDF-HFP Composite Films for Energy Storage Applications 513
 G. Himanandini and S. Narendra Babu

About the Editors

Dr. Gujjala Raghavendra has been an assistant professor in the Department of Mechanical Engineering at the National Institute of Technology Warangal, India, since 2013. He acquired the B.Tech. degree from Bapatla Engineering College, India. He completed his M.Tech. and Doctor of Philosophy (Ph.D.) in Mechanical Engineering from the National Institute of Technology Rourkela, India. He has published 140 papers in respected international journals, 16 book chapters, one book, and four granted patents and is the recipient of several awards and accolades at international/national levels for his excellence in research and academics. One project in DST SERB under ECR was successfully completed worth of 37 lakhs. He has guided five Ph.D. scholars and nine ongoing Ph.D. He received Young Engineer of the Year 2018 from IEI Telangana and Early Career Research Award 2016.

Dr. B. B. V. L. Deepak is currently working at the National Institute of Technology Rourkela, in the Department of Industrial Design. He received his master's and Ph.D. degrees from the National Institute of Technology Rourkela, in 2010 and 2015, respectively. He has 11 years of research and teaching experience in manufacturing and product design fields. He produced three Ph.D. theses and is supervising four Ph.D. scholars. He published more than 100 papers in various peer-reviewed journals and conferences along with one patent. He is also currently handling two sponsored research projects in the field of robotics. He received several national and international awards such as Ganesh Mishra Memorial Award 2019, IEI Young Engineer Award 2018, and Early Career Research Award 2017.

Dr. Manoj Gupta was the former head of Materials Division of the Mechanical Engineering Department and Director designate of Materials Science and Engineering Initiative at NUS, Singapore. He did his Ph.D. at University of California, Irvine, USA (1992), and postdoctoral research at University of Alberta, Canada (1992). He is currently among top 0.6% of researchers as per Stanford's List, among top 1% Scientist of the World Position by the Universal Scientific Education and Research Network, and among 1% of scientists as per ResearchGate. His international rank among Materials Researchers in the World is currently at 1305. He has also

co-authored eight books, published by John Wiley, Springer, and MRF-USA. He is an editor-in-chief/editor of twelve international peer-reviewed journals. A multiple award winner, he actively collaborates/visits Japan, France, Saudi Arabia, Qatar, China, USA, and India as a visiting researcher, professor, and chair professor.

Structural, Mechanical, and Corrosion Resistance Properties in 3.5% NaCl Solution of Electroless Deposited Ternary Ni–P–W System



Muralidharan Ramachandran, Pranay Vagad, Ramavtar Sharma, P. P. Deshpande, Ravi Bhatkal, and Dinesh Semwal

Abstract Low phosphorous electroless Ni–P coating containing W was prepared by incorporating sodium tungstate at different concentrations in a commercial low phosphorous electroless nickel bath. A total of five samples of Ni–P–W were prepared with different concentrations and compared with commercial low-P EN coating. The structure and the microstructure analysis showed Ni phase in as-plated samples and Ni and Ni₃P phase in the heat-treated samples. The results from SEM-EDS show no presence of W which was also confirmed by using ICP-OES analysis. The microhardness evaluated on the cross-section of the samples followed the standard trend of a low phosphorous coating. Potentiodynamic polarization test in 3.5% NaCl showed that the corrosion rate decreases by an order of magnitude after heat treatment at 400 °C for 1 h. Similar observation was made from the EIS studies of the as-plated and heat-treated samples. Heat treatment decreases the corrosion rate by an order of magnitude when compared to the as-plated samples.

Keywords Electroless Ni · Tungsten · Microstructure · Microhardness · Heat treatment · Corrosion resistance

1 Introduction

In recent years, electroless nickel has gained attention from researchers because of its increasing demand in various industrial applications. Properties like uniformity, wear and abrasion resistance, corrosion resistance, hardness, solder ability, and coefficient of friction make it suitable for several applications in the chemical and petrochemical,

M. Ramachandran (✉) · R. Sharma · R. Bhatkal · D. Semwal
Coventya India Pvt. Ltd./MacDermid Enthone Industrial Solutions, Pune, MH 412115, India
e-mail: Muralidharan.Ramachandran@macdermidenthone.com

P. Vagad · P. P. Deshpande
COEP Technological University, Pune, MH 411005, India

© The Author(s), under exclusive license to Springer Nature Singapore Pte Ltd. 2024
G. Raghavendra et al. (eds.), *Recent Advances in Mechanical Engineering, Volume 2*,
Lecture Notes in Mechanical Engineering,
https://doi.org/10.1007/978-981-97-2249-5_1

marine, electrical and electronics, medical and pharmaceutical, military, automotive, and aerospace industries [1]. The conventional electroless nickel-phosphorous deposition forms a coating with good adhesion to complex geometries of metallic as well as non-metallic substrates [2]. Its tuneable properties in the low P (2–5 wt.%), mid P (6–9 wt.%), and high P (10–12 wt.%) ranges can be further enhanced by the addition of ternary alloying elements or secondary phases. There are numerous literatures that have been published on the ternary Ni–P systems such as Ni–Cu–P [3, 4], Ni–Mo–P [5], Ni–W–P [6–8], Ni–Cr–P [9], and Ni–Fe–P and Ni–Fe–P–B [10]. Several rare earth additions to Ni–P bath such as Ni–La–P, Ni–Ce–P [11–13] have been reported in the literature.

Several nanomaterial-based Ni–P coatings have also been reported in the literature such as Ni–P–TiO₂ [14, 15], Ni–P–SiC and Ni–P–Si₃N₄ [16], Ni–P–CNT [17], and Ni–P–ZrO₂ [18] to name a few. These coatings have varying properties depending on the dispersion material and its concentration such as good anticorrosion property, decrease of coefficient of friction, and enhanced microhardness.

In this paper, sodium tungstate is added to a commercial NiP bath to get Ni–P–W ternary alloy coating. Tungsten and its alloys are known for mechanical, tribological, electrical, electro-erosion properties. Incorporation of tungsten in EN coating improves its wear resistance. Due to solid solution strengthening by tungsten into nickel matrix its properties like hardness and high-temperature stability are improved [19]. In literature, various authors studied properties like friction and wear behavior [2, 19, 20], corrosion resistance [2, 21–23], and hardness [2, 19–23]. This study is focused on the surface morphology, structural determination, surface hardness, and corrosion resistance of tungsten incorporated low phosphorous electroless nickel. Commonly heat treatment is conducted after electroless coating, and as per the findings of various authors, the properties improve after formation of solid solution of alloying element of the bath [2, 22, 24, 25].

2 Experimental

For the synthesis of NiP and NiPW coatings, a commercial low phosphorous chemistry from Coventya India Pvt. Ltd., ENOVA EF-243, was used. The chemistry was used as-it-is to produce NiP coatings while sodium tungstate was added at varying concentrations to produce NiPW coatings. Table 1 describes the nomenclature of the coatings and its corresponding sodium tungstate concentration.

Mild steel (MS) material of dimensions 10 cm × 7 cm × 0.1 cm was used as substrate. The substrate was cleaned and pretreated before plating in the bath. In the pretreatment process, mild substrate was subjected to de-greasing, water rinsing, pickling in 20–30% Hydrochloric acid, water rinsing, acid-dip in 5% sulfuric acid for 10 s, water rinsing, 5% ammonia dip and again followed by water rinsing. The substrate after cleaning and pretreatment was introduced into the plating bath.

The chemical composition and operating parameter of bath are shown in Table 2. Low P EN coating was also prepared using ENOVA 243 to compare with the NiPW

Table 1 Concentration of sodium tungstate used in experiments

Nomenclature	Concentration of sodium tungstate (g/L)
NiP	0
NiPW2	2
NiPW5	5
NiPW10	10
NiPW20	20
NiPW50	50

Table 2 Chemical composition and operating parameter of bath

Chemical composition and operating parameter	Concentration and parameter value
Ni metal concentration	6 g/L
Na hypophosphite concentration	24 g/L
Bathing loading	1.0 dm ² /L
Sodium tungstate (g/L)	2, 5, 10, 20, and 50
Temperature of bath	88 °C
Operating pH of bath	6.2

samples. The thickness of the coating ranged from 50 to 60 μm calculated by gravimetric technique. The prepared sample was cut into eight pieces by sheet cutting bench shearing machine. One cut piece from each composition of NiPW was annealed at 400 °C for 1 h. The as-plated and heat-treated samples were tested for structural, microstructural, mechanical, and corrosion properties using various techniques.

Structural characterization was carried out using a Bruker D8 Advance, XRD (Germany) with $\text{CoK}\alpha$ radiation (wavelength = 1.7889 Å) at an accelerating voltage of 35 kV and 40 mA. Microstructural characterization was done using a scanning electron microscope (SEM) from Carl ZEISS (Model: Sigma HV) fitted with energy dispersive spectrometer (EDS).

Mechanical property (hardness) was tested using a microhardness tester (Model: FM-700, Future Tech Corp., Tokyo, Japan). Corrosion studies were performed using a potentiostat/galvanostat (Model: Gamry Reference 1000, Wilmington, USA).

3 Results

3.1 Deposition Rate

The plating rate of the processes was measured using gravimetric technique. The weight of the panel was noted before and after plating. Based on the weight gained during the plating process, the plating rate was calculated.

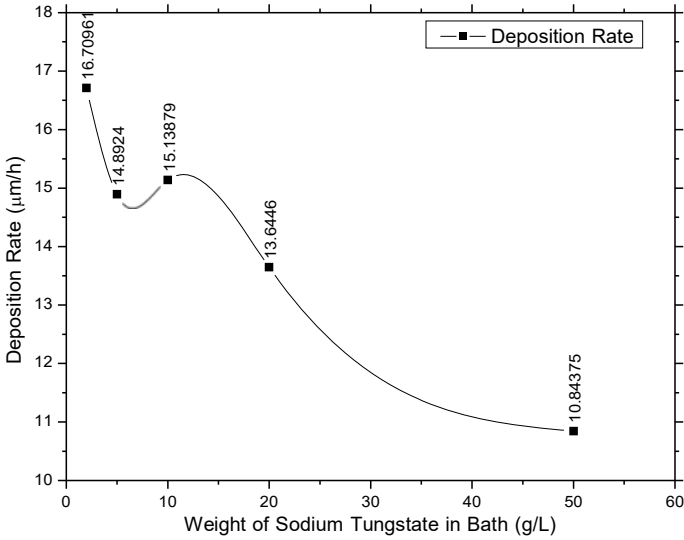


Fig. 1 Variation of plating rate ($\mu\text{m/h}$) with respect to the weight of sodium tungstate in bath (g/L)

It can be seen from Fig. 1 that the plating rate decreases with an increase in the amount of sodium tungstate in the bath. An almost linear trend was observed in the reduction in the plating rate with the increase in amount of sodium tungstate. It is also important to mention here that the finish of the plated panels was much smoother at lower concentration of sodium tungstate in the bath which became rougher with the increase in sodium tungstate concentration.

3.2 Phase Analysis

XRD patterns of the as-plated panels show the presence of only peaks that correspond to Ni (PCPDF # 01-088-2326) [26] as shown in Fig. 2. It is evident, from the XRD patterns shown for various concentrations of sodium tungstate additions, that the major orientation of the Ni is along the (111) direction. We also see the peaks along the (200) and (220) directions. The actual material that is present is an alloy of Ni and P.

Figure 3 shows the diffraction pattern of the heat-treated samples of NiPW. It can be seen from the XRD patterns that the heat-treated material is a combination of Ni and Ni_3P phases. It is confirmed by matching the peaks of PCPDF # 01-088-2326 [26] for Ni phase and PCPDF # 00-034-0501 [26] for Ni_3P phase.

Lattice parameter calculations were done using the following equation:

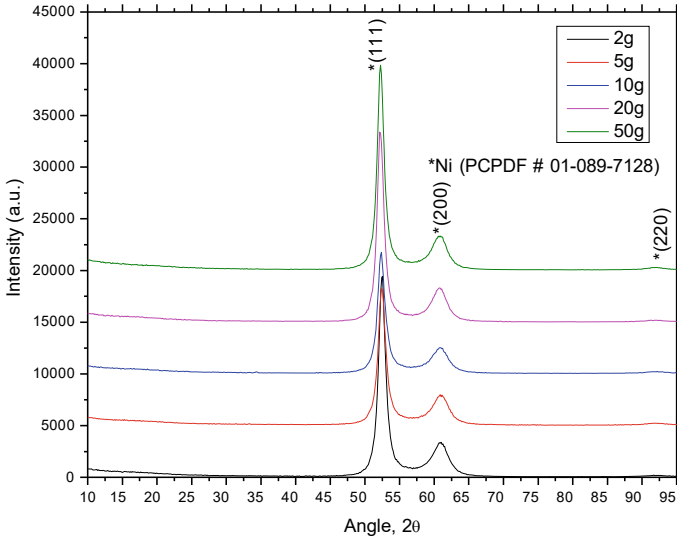


Fig. 2 XRD of as-plated samples of NiPW

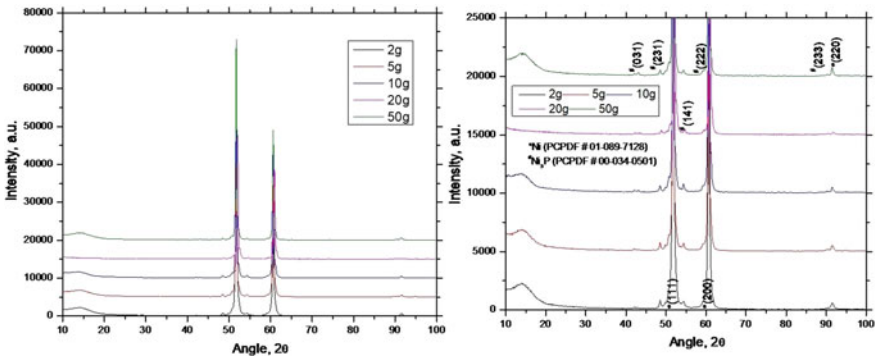


Fig. 3 XRD of heat-treated samples (left) and (zoomed-right) samples of NiPW

$$\frac{1}{d^2} = \frac{h^2 + k^2 + l^2}{a^2} \text{ for cubic and } \frac{1}{d^2} = \frac{h^2 + k^2}{a^2} + \frac{l^2}{c^2} \text{ for tetragonal} \quad (1)$$

where d is the interplanar d -spacing in Å; (hkl) corresponds to the crystal orientation, and a is the lattice parameter in Å. Crystallite size was determined by using Debye-Scherrer equation [27–29].

The fact that the material that is deposited is an alloy of Ni and P is evident from the lattice parameter calculations shown in Fig. 4. The lattice parameter, a , for pure Ni is 3.535. But there is a variation, specifically a decrease in the lattice parameter

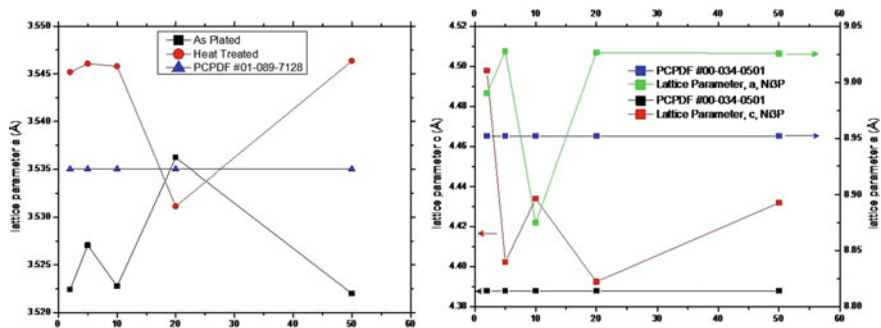


Fig. 4 Lattice parameter calculation from XRD data for Ni (left) and Ni₃P (right) phase

values with the addition of sodium tungstate. Only in the case of NiPW20, the lattice parameter is close to that of pure Ni.

It can also be observed from Fig. 4 that the lattice parameter, *a*, of heat-treated samples was higher than that of pure Ni. This is true for all the samples with addition of sodium tungstate. In the case of NiPW20, though, the lattice parameter was very close to that of pure Ni.

There is no specific trend seen from the amount of sodium tungstate addition to the plating bath on the variation of lattice parameter. It can still be concluded that the optimum solid solution is possible at a sodium tungstate addition of 20 g/L, where the distortion of the lattice is minimum. Further addition of sodium tungstate to the bath such as 50 g/L reduces the lattice distortion but again results in much rougher plated part. This could mean that the W that is co-deposited is not going into a solid solution with the NiP matrix.

The XRD data of heat-treated samples were analyzed for the lattice parameter variation of the Ni₃P phase. It was observed that the composition NiPW20 is the optimum in this case as well as can be seen from Fig. 4. The lattice parameter was highly distorted at other compositions but in NiPW20, both *a* and *c* of the tetragonal lattice were closer to that of pure Ni₃P.

The crystallite size calculated for the as-plated samples shows minimum crystallite size for NiPW20 sample. It was also observed that in the heat-treated samples, it was the opposite trend where the NiPW20 sample had the maximum crystallite size. The trend of change in crystallite size with change in sodium tungstate concentration is shown in Fig. 5. The crystallite size of the as-plated samples varied between 1.5 and 2 Å, while that of the heat-treated samples varied between 4 and 5 Å.

Phase analysis of the heat-treated material was done using XRD. The volume fraction calculation was done using direct comparison method [30]. The procedure to obtain volume fraction is described elsewhere [31]. An analysis of the phases in the heat-treated material shows that the amount of Ni₃P phase decreases with an increase in the sodium tungstate concentration in the bath as shown in Fig. 5.

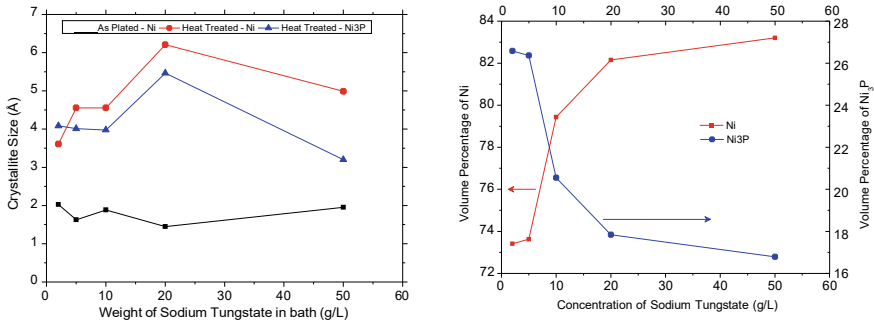


Fig. 5 Crystallite size from XRD data for Ni and Ni₃P phases (left); volume percent of Ni and Ni₃P phases in heat-treated samples

3.3 Microstructure and Elemental Analysis

The microstructure of the NiP- and NiPW-coated samples was tested using scanning electron microscopy (SEM). As expected from electroless nickel plating, it was found that the microstructure of NiP and NiPW alloys was all cauliflower-like. The microstructure of the coated samples from NiPW10 is shown below at two different magnifications, i.e., 500 \times and 1000 \times in Fig. 6. It was also observed that there were no pores or openings in the coating, suggesting a good barrier coating on top of the MS panels. Hence, this type of coating is supposed to provide relatively good corrosion protection of the base material.

Further, the samples from the SEM analysis were also analyzed using elemental dispersive spectroscopy (EDS) in the SEM instrument. One of the main observations from the analysis was that there was no W observed in the coating in all the samples, i.e., NiPW2, NiPW5, NiPW10, NiPW20, and NiPW50.

To ensure that the analysis was correct, thin film foils were obtained from these coatings. A small portion of these films was first weighed and then dissolved in dilute nitric acid. The dissolved solution was then made up to a specific volume, and then the solution was analyzed using ICP-OES. It was found that in all the samples, i.e., NiP2, NiPW5, NiPW10, NiPW20, and NiPW50, the content of W was very minimal and was found in ppm levels as shown in Table 3.

It was a surprising fact that the addition of sodium tungstate didn't incorporate W into the coating. It acted as a stabilizer reducing the plating rate with the increase in the sodium tungstate content. The reduction of plating rate with increase in the sodium tungstate content has been given in Fig. 1.

Figure 7 shows the relative percentages of Ni, P, and W in the coating. As explained earlier there was no W found in the coatings. As the proprietary chemical obtained from Coventya India Pvt. Ltd. was a low phosphorous chemistry, the content of P was about 2.45 wt.% as can be observed from Fig. 7. Another interesting finding is that the amount of P content (in wt.%) steadily decreased with an increase in the content of sodium tungstate in the bath. This is clearly depicted in the graph shown

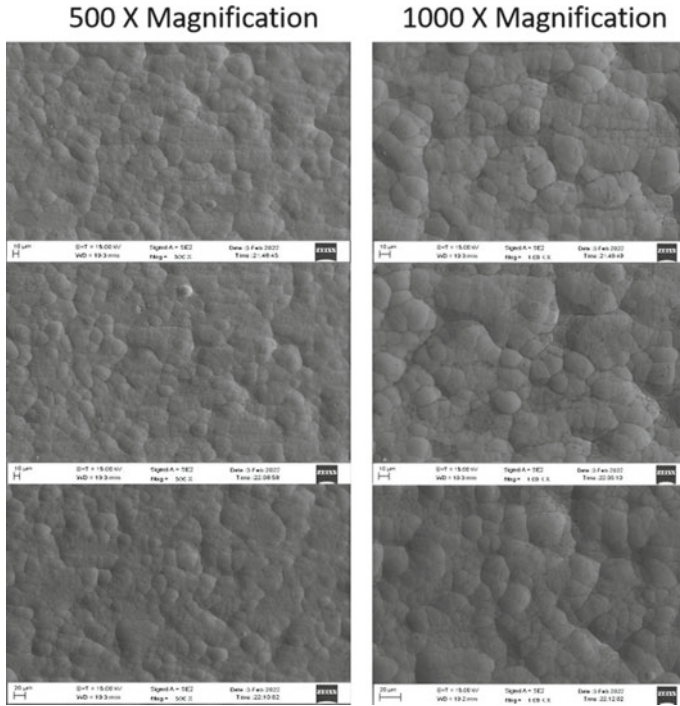


Fig. 6 SEM of NiPW10 at magnifications of 500× and 1000×

Table 3 ICP analysis results for NiPW systems

Sample	Tungsten (in %)
NiPW2	0.061
NiPW5	0.09
NiPW10	0.06
NiPW20	0.026
NiPW50	0.081

in Fig. 7. This was also seen in the volume percent analysis of the phases from XRD where the concentration of the Ni₃P phase decreased with the increase in the sodium tungstate concentration in the bath (Fig. 5).

3.4 Hardness

The as-plated hardness of the NiP system was about 660 HV_{0.05} as can be seen in Fig. 8. The indentation was formed on the cross-section of the coating as can be

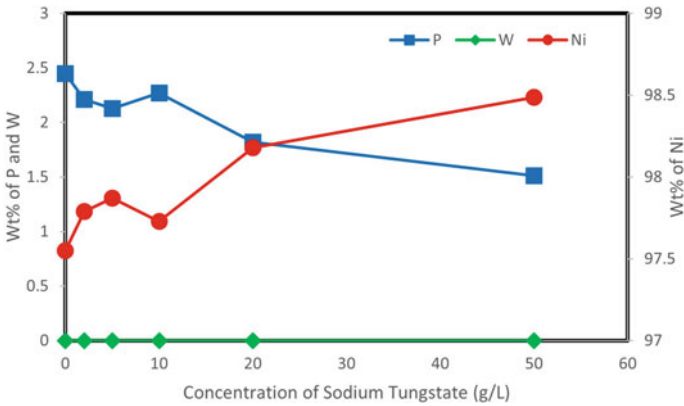


Fig. 7 Wt.% of elements in the coating at various concentrations of sodium tungstate addition

seen from the inset in Fig. 8. Many a times, the indentation doesn't form a perfect diamond shape with equal diagonals. In such case, the readings must be retaken. The heat treatment was done at 400 °C for a time of 1 h. This led to the formation of Ni₃P phase as was seen in the XRD of the heat-treated samples. The formation of Ni₃P phase increases the hardness, and it was about 900 HV_{0.05}.

In the case of NiPW, the maximum hardness was achieved in the NiPW20 sample in both the as-plated and the heat-treated samples. The as-plated hardness was about 693 HV_{0.05}, while that of heat-treated sample was about 942 HV_{0.05}. In general,

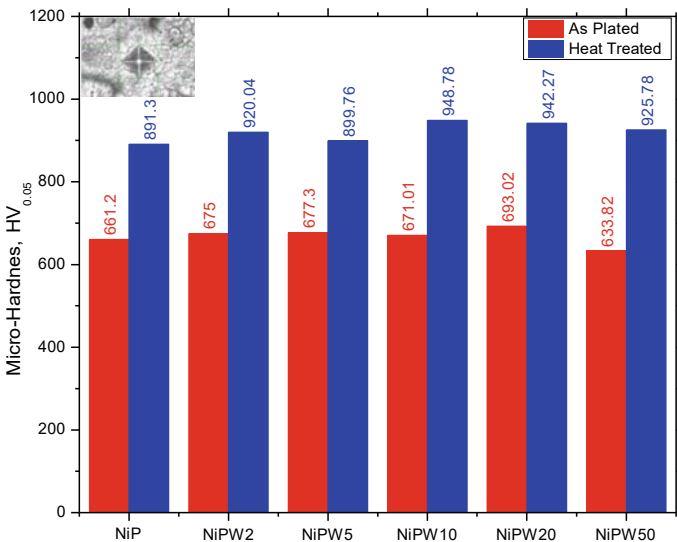


Fig. 8 Indentation formed on the cross-section of the coating during hardness testing (inset); effect of heat treatment temperature and W concentration on the hardness of the plated panels

both the binary NiP system and the ternary NiPW systems follow the same trend of hardness in the as-plated and the heat-treated samples except for a marginal change.

3.5 Corrosion Resistance in 3.5% NaCl

3.5.1 Potentiodynamic Polarization Test

The test coupons were plated with NiPW and were tested using potentiostat/galvanostat instrument. From the graphs obtained during the testing, I_{corr} and E_{corr} were obtained. This is tabulated in Table 4. The corrosion rate in mpy was also determined based on the I_{corr} values obtained. It can be seen from the table that the corrosion rate is in general higher for the as-plated samples compared to the heat-treated samples in the case of NiPW5 and NiPW10. This is due to the formation of Ni₃P phase in the heat-treated samples. The corrosion current was very low for the NiPW2 sample which led to lower corrosion rate. It is also noted in the NiPW2 sample that the corrosion rate for the heat-treated sample was higher than the as-plated samples.

Figure 9 shows polarization curves for as-plated NiPW samples and heat-treated NiPW samples in 3.5 mass% NaCl solution. The corrosion potential, corrosion current densities, and corrosion rate values are tabulated in Table 4. For the NiPW2 sample, corrosion potential shifted from -582 mV for an as-plated sample to -479 mV for a heat-treated sample. Table 4 revealed that the corrosion potential of heat-treated samples was more noble (positive) than that of as-plated samples. The positive shift indicates an anodic protection mechanism in the case of heat-treated samples. The corrosion rate for heat-treated samples was significantly lower than that of the as-plated samples owing to the formation of Ni₃P phase in the heat-treated samples. When compared to NiPW5 and NiPW10 samples, the corrosion rate for NiPW2 samples is significantly lower.

Table 4 Potentiodynamic polarization test on NiPW-coated samples

Sample		I_{corr}	E_{corr} (mV)	Corrosion rate (mpy)
NiPW2	As-plated	21.40 nA	-582.0	0.005
	Heat-treated	50.40 nA	-479.0	0.002
NiPW5	As-plated	260.0 μ A	-521.0	36.14
	Heat-treated	30.40 μ A	-461.0	3.253
NiPW10	As-plated	190.0 μ A	-534.0	26.39
	Heat-treated	31.30 μ A	-456.0	3.352

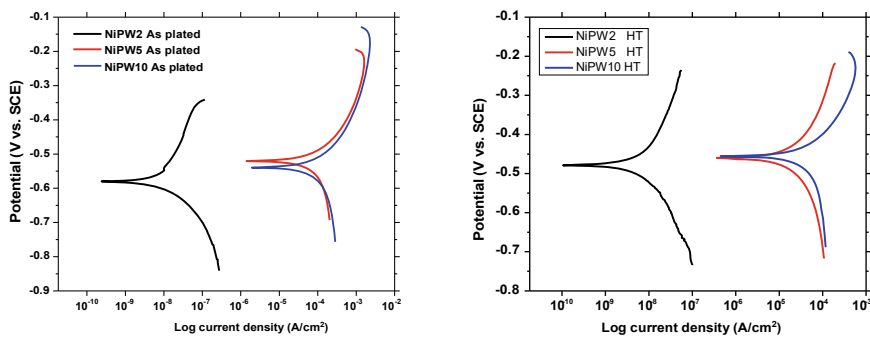


Fig. 9 Tafel plots for NiPW as-plated (left) and NiPW10 heat-treated (right) samples

3.5.2 Electrochemical Impedance Spectroscopy

EIS measurements were made on the samples coated with NiPW. These measurements, in terms of Bode and Nyquist plots, are depicted in Figs. 10 and 11. The Z_{mod} and Z_{real} values were determined from the Bode and Nyquist plots, respectively.

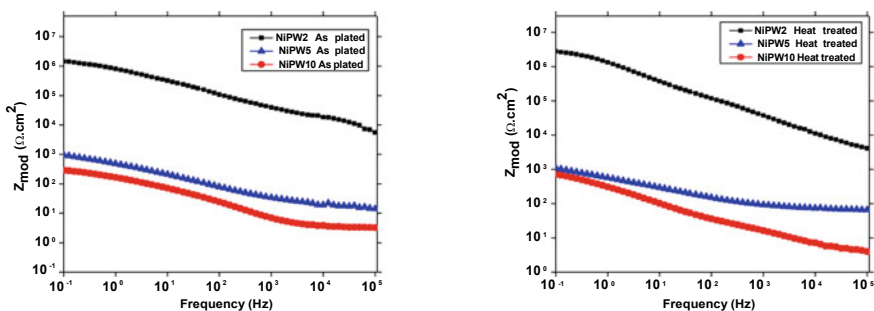


Fig. 10 Bode plot for NiPW as-plated (left) and heat-treated (right) samples

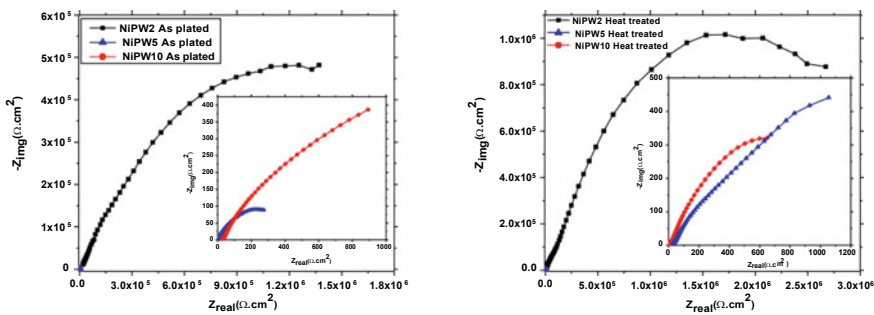


Fig. 11 Nyquist plot for NiPW as-plated (left) and heat-treated (right) samples

The electrochemical impedance spectra were modeled using equivalent circuit shown in Fig. 12. It consists of the coating capacitance C_c , the coating resistance R_c , the double layer capacitance C_{dl} , and the charge transfer resistance R_{ct} . All impedance values obtained from the Bode and Nyquist plots by using an equivalent circuit are recorded in Table 5.

In the Bode plots, the high-frequency and low-frequency portions correspond to capacitive and resistive behavior, respectively (Fig. 10). The impedance (Z_{mod}) value of the NiPW2 sample is enhanced from $1452 \text{ k}\Omega \text{ cm}^2$ for the as-plated sample to $2811 \text{ k}\Omega \text{ cm}^2$ for the heat-treated sample. Similarly, impedance (Z_{mod}) values for heat-treated NiPW5 and NiPW10 samples are higher than for as-plated samples. Higher impedance values (Z_{mod} and Z_{real}) are seen in the NiPW2 samples than in the NiPW5 and NiPW10 samples.

In the case of coated mild steel, corrosion resistance can be estimated by the addition of charge transfer resistance and coating resistance [32]. The corresponding values for the as-plated NiPW2, NiPW5, and NiPW10 samples were $1083 \text{ k}\Omega \text{ cm}^2$, $873.9 \text{ }\Omega \text{ cm}^2$, and $214.68 \text{ }\Omega \text{ cm}^2$, respectively. Corrosion resistance values for NiPW2, NiPW5, and NiPW10 samples in the case of heat-treated samples were

Fig. 12 Equivalent circuit used for modeling impedance curves

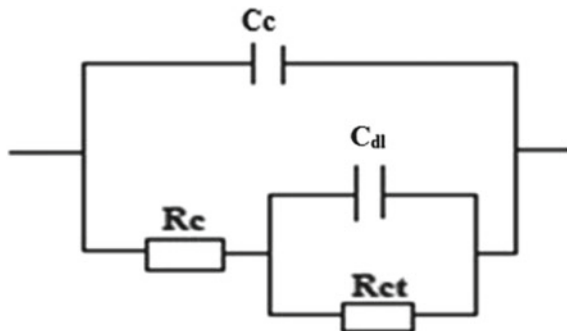


Table 5 Impedance values obtained from Bode and Nyquist plots

Sample		$Z_{real} (\Omega \text{ cm}^2)$	$Z_{mod} (\Omega \text{ cm}^2)$	$R_{ct} (\Omega \text{ cm}^2)$	$C_{dl} (\text{F})$	$R_c (\Omega \text{ cm}^2)$	$C_c (\text{F})$
NiPW2	As-plated	1370×10^3	1452×10^3	1.84×10^5	1.02×10^{-8}	8.99×10^5	1.07×10^{-8}
	Heat-treated	2671×10^3	2811×10^3	9.66×10^4	3.338×10^{-9}	1.85×10^6	5.66×10^{-8}
NiPW5	As-plated	893	959.5	370.3	1.71×10^{-5}	503.6	7.06×10^{-5}
	Heat-treated	1055	1089	652.2	9.36×10^{-7}	420.9	6.06×10^{-4}
NiPW10	As-plated	274.7	288.6	42.68	4.51×10^{-5}	172	4.86×10^{-4}
	Heat-treated	649.3	724.2	27.49	9.02×10^{-6}	407.1	2.41×10^{-4}

1946.6 $\text{k}\Omega \text{ cm}^2$, 1073.1 $\Omega \text{ cm}^2$, and 434.59 $\Omega \text{ cm}^2$, respectively. As capacitance depends upon the area, the lower values of coating capacitance shown by the heat-treated sample as compared to the as-plated samples indicate less electrochemical degradation. Higher impedance, coating resistance, charge transfer resistance values, and the lowest values of coating capacitance in the case of the heat-treated samples revealed its higher electrochemical resistance ability as compared to as-plated samples owing to the formation of the Ni_3P phase. These findings support the potentiodynamic polarization results.

4 Conclusion

An effort was made to obtain tungsten incorporated NiP coatings. The W incorporation was not happening in this acidic medium of the electroless nickel bath. This was confirmed by EDS and ICP-OES results. In NiPW coating baths, increasing the concentration of sodium tungstate decreases the plating rate. Increase in cross-sectional hardness was observed after heat treatment similar to that of NiP coatings. XRD of NiPW coating show the presence of nickel phosphide (Ni_3P) phase after heat treatment. SEM images of NiPW show uniform coating without any discontinuity or cracks. It was observed from the EDS results of NiPW-coated samples that an increase in sodium tungstate concentration in bath reduces the phosphorus content. ICP-OES results confirm the presence of tungsten in the coating in small amounts (0.1–0.05%). Potentiodynamic polarization test shows that the corrosion rate increases with increase in tungstate content. The corrosion rate decreases around an order of magnitude after heat treatment.

Acknowledgements Authors express their sincere thanks to Coventya India Pvt. Ltd./MacDermid Enthone Industrial Solutions for permitting to carry out the work at their premises. Authors also express their sincere thanks to the Head, Department of Metallurgy and Materials Engineering for extending facilities for this work and Hon. Vice Chancellor, COEP Technological University, Pune 411005 (M.S.), India, for his encouragement.

References

1. Agarwala RC, Agarwala V (2003) Electroless alloy/composite coatings: a review. *Sādhanā* 28(3–4):475–493
2. de Oliveira MCL, Correa OV, Ett B, Sayeg IJ, de Lima NB, Antunes RA (2018) Influence of the tungsten content on surface properties of electroless Ni–W–P coatings. *Mater Res* 21(1):1–13
3. Xu Y, Zou Y, Luan T (2013) The effect of Cu content on the properties and electrochemical behavior of electroless Ni–Cu–P coatings. *J Funct Mater* 44(2):244–248
4. Aal AA, Aly MS (2009) Electroless Ni–Cu–P plating onto open cell stainless steel foam. *Appl Surf Sci* 255(13–14):6652–6655
5. Nie S, Yang Z, Cai X, Chen Q (2003) Stress and corrosion performance of amorphous Ni–Mo–P electroless deposits. *J Funct Mater* 34(5):585–588, 591

6. Tien S-K, Duh J-G, Chen Y-I (2004) Structure, thermal stability and mechanical properties of electroless Ni–P–W alloy coatings during cycle test. *Surf Coat Technol* 177–178:532–536
7. Wu FB, Tien SK, Chen WY, Duh JG (2004) Microstructure evaluation and strengthening mechanism of Ni–P–W alloy coatings. *Surf Coat Technol* 177–178:312–316
8. Geng BS, Wie YH, Hou LF, Li S, Yang HY, Xu BS (2009) Study on the microstructure and properties of electroless Ni–W–P plating on stainless steel. *Rare Metal Mater Eng* 38(S1):71–75
9. Xiao Z, Long Y, Zhong P, Huang CH (2003) Electroless nickel–chromium–phosphorus alloy process. *Surf Technol* 32(2):47–49, 56
10. Wang LL, Zhao LH, Huang GF, Yuan XJ, Zhang BW, Zhang JY (2000) Composition, structure and corrosion characteristics of Ni–Fe–P and Ni–Fe–P–B alloy deposits prepared by electroless plating. *Surf Coat Technol* 126(2–3):272–278
11. Ashassi-Sorkhabi H, Moradi-Haghighi M, Hosseini MG (2008) Effect of rare earth (Ce, La) compounds in the electroless bath on the plating rate, bath stability and microstructure of the nickel–phosphorus deposits. *Surf Coat Technol* 202(9):1615–1620
12. Zhu Y, You L, Song TT (2011) *Electroplat Finish* 30:20–22
13. Balaraju JN, Chembath M (2012) Electroless ternary NiCeP coatings: preparation and characterisation. *Appl Surf Sci* 258(24):9692–9700
14. Song LZ, Li J, Wang FJ (2002) *Mater Sci Technol* 10:148–151
15. Petrova M, Noncheva ZB, Petrov C, Schmidt C (2000) Electrolessly deposited nickel dispersion layers on plastics: part II: nanoscale dispersoids. *Galvanotechnik* 91:3378–3384
16. Sarret M, Müller C, Amell A (2006) Electroless NiP micro- and nano-composite coatings. *Surf Coat Technol* 201(1–2):389–395
17. Zarebidaki A, Allahkaram S-R (2011) Effect of surfactant on the fabrication and characterization of Ni–P–CNT composite coatings. *J Alloys Compd* 509(5):1836–1840
18. Gay P-A, Limat JM, Steinmann P-A, Pagetti J (2007) Characterisation and mechanical properties of electroless NiP–ZrO₂ coatings. *Surf Coat Technol* 202(4–7):1167–1171
19. Kundu S, Das SK, Sahoo P (2019) Friction and wear behavior of electroless Ni–P–W coating exposed to elevated temperature. *Surf Interfaces* 14:192–207
20. Palaniappa M, Seshadri SK (2008) Friction and wear behavior of electroless Ni–P and Ni–W–P alloy coatings. *Wear* 265(5–6):735–740
21. He FJ, Fang YZ, Jin SJ (2014) The study of corrosion–wear mechanism of Ni–W–P alloy. *Wear* 311(1–2):14–20
22. Balaraju JN, Selvi VE, Grips VKW, Rajam KS (2006) Electrochemical studies on electroless ternary and quaternary Ni–P based alloys. *Electrochim Acta* 52(3):1064–1074
23. Liu H, Viejo F, Guo RX, Glenday S, Liu Z (2010) Microstructure and corrosion performance of laser-annealed electroless Ni–W–P coatings. *Surf Coat Technol* 204(9–10):1549–1555
24. Balaraju J, Sankara Narayanan T, Seshadri S (2001) Evaluation of the corrosion resistance of electroless Ni–P and Ni–P composite coatings by electrochemical impedance spectroscopy. *J Solid State Electrochem* 5(5):334–338
25. Ansari A, Ram M, Sharma S, Sharma AK (2020) Development of electroless Ni–P/W nanocomposite coatings and its microhardness. *AIP Conf Proc* 2297(1):020001
26. Powder Diffraction File-4 (PDF-4) (2011) International centre for diffraction data (ICDD). Joint Committee on Powder Diffraction Standards (JCPDS)
27. Patterson AL (1939) The diffraction of X-rays by small crystalline particles. *Phys Rev* 56:972–977
28. Patterson AL (1939) The Scherrer formula for X-ray particle size determination. *Phys Rev* 56:978–982
29. Boswell FWC (1951) Precise determination of lattice constants by electron diffraction and variations in the lattice constants of very small crystallites. *Proc Phys Soc A* 64:465–478
30. Cullity BD (1978) *Elements of X-ray diffraction*, 2nd edn. Addison-Wesley Publishing Co.
31. Ramachandran M (2012) *Thermal plasma processing of fine grained materials*. Ph.D. dissertation, University of Alabama
32. Deshpande P, Vagge S, Jagtap S, Khiarnar R, Kelkar S, More M (2012) Conducting polyaniline based paints on hot dip galvanized low carbon steel for corrosion protection. *Bulg Chem Commun* 44(4):318–323

Dry Ice Cooling Effect on Friction Stir Welded AA6061 Alloy Using Brass Interlayer



Korra Nagu and Adepu Kumar

Abstract This study investigated the impact of employing dry ice cooling and a brass interlayer on the metallurgical and mechanical behavior of AA6061 welded alloy. Friction stir welding (FSW) is commonly used to weld Al alloys as an alternative to the fusion welding process. Generally, FSW leads to the formation of recrystallized and refined grains in comparison to base metal. Despite the presence of grain refinement in the stir zone without an interlayer, the material experienced a reduction in strength due to thermal softening. The addition of a brass interlayer in between the welds during FSW produced strong metallurgical intermetallics. The production of strengthening metallurgical intermetallics enhanced weld mechanical properties with interlayer. However, strength recovery was not achieved in the heat-affected zone with normal cooling. Furthermore, premature failure was caused by the formation of brittle and hard intermetallics in the weld's stir zone containing the interlayer. Therefore, dry ice cooling was employed to increase the hardness in the heat-affected zone and the overall strength of the weld. Dry ice cooling with the interlayer reduced heat-affected zone softening and enhanced hardness. Moreover, by employing dry ice cooling in conjunction with the interlayer, the formation of hard intermetallics was inhibited, and the volume of intermetallics was significantly reduced due to the rapid cooling rate. As a result, the overall strength of the weld joint was increased from 247 MPa with normal cooling to 268 MPa with dry ice cooling.

Keywords Dry ice cooling · Natural cooling · Friction stir welding · Brass interlayer · Intermetallics

K. Nagu (✉)

Mechanical Engineering Department, B V Raju Institute of Technology, Narsapur,
Telangana 502313, India
e-mail: nagu.k@bvr.it.ac.in

A. Kumar

Mechanical Engineering Department, National Institute of Technology, Warangal, Warangal,
Telangana 506004, India

1 Introduction

Aluminum alloys are widely utilized in the aerospace and automobile industries, mainly due to their high strength and comparatively moderate density [1]. The most used friction stir welding (FSW) as solid-state welding procedure overcomes the difficulty of welding Al alloys with fusion welding processes [2]. The FSW procedure comprises when a rotating tool penetrates at the abutting edges of two weld materials, due to the shoulder's shearing action and high normal pressure, and frictional heat is primarily produced. The tool transverse along the line joining can transport the material from one side to another side which will be carried forward and rotated around the pin. Consequently, at the rear of the retreating side, there is an accumulation of material resulting in forming the weld joint. Hence, the movement and rotation of the material facilitated the bonding and consolidation of the weld pieces, resulting in a robust and seamless weld [3]. As a result of the dynamic recrystallization process and the intense deformation of the material during FSW, the weld joint's stir zone exhibits the presence of small, equiaxed grains [4]. Even though FSW was utilized to produce fine and recrystallized grains, the softening at the SZ brought on by the weld heat cycle reduces the strength of the weld joint [5, 6]. Hence, there is a need to enhance the weld joint strength. Moreover, numerous researchers have attempted to increase the weld joint strength through tool design, FSW parameters optimization, and post-weld heat treatment [7]. The aforementioned processes are not highly effective methods, as they may require additional time for the design and fabrication of tools, lead to wastage of base material, and involve significant costs for optimization, ultimately diminishing the overall welding economy. A few researchers have proposed introducing an appropriate interlayer between weld plates to overcome the aforementioned challenges and enhance joint strength. A soft material such as Zn was used as an interlayer to weld Al7020 alloy using FSW by Wilson et al. [8]. They carried out the research by varying the thickness with constant composition of interlayer material. The researchers described that a Zn interlayer with a thickness of 100 μm enhanced mechanical properties more than other interlayers. This improvement can be attributed to the effective diffusion of Zn particles within the Al matrix, leading to enhanced grain refinement. The researchers' Mokabberi et al. [9] investigation focused on three different interlayer materials (Cu, Zn, and brass) having varying hardnesses on metallurgical mixing and enhancement of mechanical properties. The findings revealed that the utilization of brass interlayers led to improved mechanical properties. This enhancement was attributed to the intermixing reaction between the aluminum matrix and brass particles, forming robust intermetallic compounds (IMCs) through the distribution and diffusion of brass particulates. A single interlayer (Cu) with high hardness and heat treatment to form a good metallurgical bond with aluminum base metal was used by Khojastehnezhad et al. [10]. They concluded that the synthesis of Al_4Cu_9 and Al_2Cu intermetallics increased the weld's mechanical properties. The mechanical properties can be enhanced attributed to lower the thickness of intermetallics. Cooling rate plays a vital role in reducing the thickness of intermetallics and in forming a strong metallurgical bond. Moreover, the cooling rate

in FSWed dissimilar welds or welds with interlayer results in reduced intermetallics, which can form strong metallurgical bonds between interlayer particles and the Al matrix. This strong bond formation leads to an enhancement in the tensile strength of the overall weld joint [11, 12]. Even though Çam et al. [13] employed external cooling simultaneously with a high-strength interlayer to enhance weld strength, no improvements were observed in microstructural and mechanical properties. Nevertheless, the researchers recommend the use of external cooling as a means to enhance weld performance. Additionally, some researchers have directed their attention toward achieving very rapid cooling rates, such as with liquid nitrogen or dry ice, to improve weld properties. Bansal et al. [14] performed FSW using a speedy cooling rate, including deep cryogenic treatment. The researchers noted that rapid cooling increased grain refinement, improving mechanical properties like toughness and strength. This observation highlights the positive impact of fast cooling on enhancing the overall quality and performance of the weld. Liu et al. [15] investigated the impact of liquid oxygen (O_2) on the mechanical properties and microstructural characteristics of FSWed aluminum alloy. They observed the influence of rapid cooling rates on the sharpening of textures in welds, reduced grain growth, and improved mechanical properties. Generally, a faster cooling rate possesses higher specific heat compared to normal cooling. Furthermore, it has demonstrated tremendous promise for enhancing ductility and mechanical properties [16]. In addition, the rapid cooling process can effectively reduce the tensile residual stresses within the weld zone. This reduction in residual stresses is highly advantageous for enhancing the fatigue performance of the joints. By minimizing these stresses, the weld joints become more resistant to fatigue failure, thereby increasing their durability and reliability [17].

According to existing literature, faster cooling significantly affects metallurgical properties, reducing the formation of IMCs in the SZ of FSWed joints. Based on the available literature, there is a need for further investigation into the combined effect of very rapid cooling methods, such as dry ice, and the utilization of an interlayer on the metallurgical behavior and mechanical properties of AA6061 welded using friction stir welding. In contrast to naturally cooled FSW joints, this specific combination has yet to be extensively studied or documented. By employing brass as the interlayer, this study aims to enhance the mechanical properties and microstructural characteristics of dry ice-cooled AA6061 weld joints.

2 Materials and Methods

The weld material utilized in the current investigation consists of AA6061-T6 plates with a thickness of 6 mm. A brass interlayer, composed of 58% Cu and 36% Zn (0.2 mm thin), was taken as the interlayer material. The welding procedure was done with the help of a cylindrical profiled tool with left-hand threads (Fig. 1a). Figure 1b depicts the placement of the brass interlayer positioned between the two weld plates, and Fig. 1c depicts the actual FSW process. Tool rotational speed of 800 rpm, tool penetration depth of 0.2 mm, and traverse speed of 25 mm/min are used in this study.

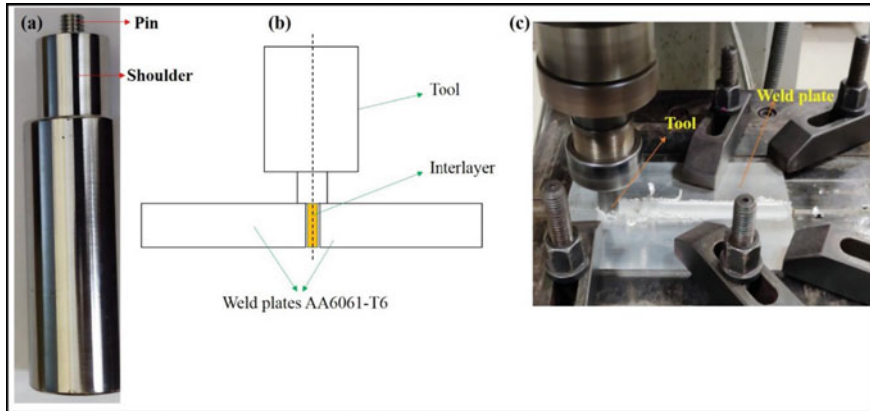


Fig. 1 a Cylindrical profiled tool with threading, b representation of FSW with interlayer, and c actual welding process

The welding process was conducted in four distinct phases to enable a comparative and detailed analysis of the cooling's impact. This phased approach allowed for a comprehensive examination of how different cooling conditions affected the evolution of IMCs and precipitates within the weld joint. Natural cooling: without interlayer (NCWO) and with interlayer (NCWI); dry ice cooling: without interlayer (DIWO) and with interlayer (DIWI). For DIWO and DIWI welding, the dry ice cooling treatment was applied immediately after FSW along the traverse line of the tool.

To attain a proper finish on the microstructural weld materials, they were initially sliced in a perpendicular direction to the weld. Subsequently, they underwent polishing using various grades of SiC sheets. Following the polishing process, the samples were etched in an etchant. Both a scanning electron microscope (SEM) and a three-dimensional optical microscope (OM) were employed for microstructure investigation. The weld joint's hardness was assessed using a Vickers hardness testing machine, applying an indentation force of 100 g for 10 s, and maintaining a spacing of 0.5 mm between each indentation. By the ASTM-E8 standard, samples intended for the tension test were cut across the weld direction. A universal testing machine (UTM) was utilized to perform the tension test, and the average of three sample results was calculated to obtain a representative measurement.